



*Republic of Iraq  
Ministry of Higher Education &  
Scientific Research  
University of Diyala  
College of Science  
Department of Physics*



# **Synthesis of Some Ternary Metal Oxides and Sulphides Nanostructures Thin Films For Photovoltaic Applications**

A thesis

Submitted to the Council of the College of Science  
University of Diyala in Partial Fulfillment of Requirements  
for the Degree of Doctor of Philosophy in Physics sciences

By

**Layth Ali Saleh**

B.Sc. in Physics, 2003

M.Sc. in Physics, 2016

Supervised By

**Prof. Dr.  
Ziad T. Khodair**

2022 A.D.

1444 A.H.

# بِسْمِ اللَّهِ الرَّحْمَنِ الرَّحِيمِ

هُوَ الَّذِي جَعَلَ الشَّمْسَ ضِيَاءً وَالْقَمَرَ نُورًا

وَقَدَرَهُ مَنَازِلَ لِتَعْلَمُوا عَدَدَ السِّنِينَ

وَالْحِسَابِ مَا خَلَقَ اللَّهُ ذَلِكَ إِلَّا بِالْحَقِّ

يُفَصِّلُ الْآيَاتِ لِقَوْمٍ يَعْلَمُونَ ﴿5﴾

صدق الله العظيم

## Supervisors Certification

We certify that this thesis entitled “*Synthesis of Some Ternary Metal Oxides and sulphides Nanostructures Thin Films for Photovoltaic Applications*” for the student (Layth Ali Saleh), was prepared under our supervisions at the Department of Physics, College of Science, University of Diyala in partial fulfillment of requirements needed to award the degree of *Doctor of Philosophy (Ph.D.) of Science in Physics*.

**Signature:**

**Name: Dr. Ziad Tariq Khodair**

**Title: Professor**

**Address: College of Science,**

**University of Diyala**

**Date:    /    / 2022**

### **Head of the Physics Department**

**In view of available recommendation, I forward this thesis for debate by the examining committee.**

**Signature:**

**Name: Dr. Ammar Ayesh Habeeb**

**Title: Assistant Professor**

**Head of the Physics Department**

**Address: College of Science, University of Diyala**

**Date:    /    / 2022**

## **Scientific Amendment**

**I certify that the thesis entitled " *Synthesis of Some Ternary Metal Oxides and sulphides Nanostructures Thin Films for Photovoltaic Applications* " presented by student (Layth Ali Saleh) has been evaluated scientifically, therefore, it is suitable for debate by examining committee.**

### **Signature**

**Name: Widad H . Abbas**

**Title: Assistant Professor**

**Address: Al-Mustansiriyah University, College of Basic Education, Science Department**

**Data:     /     / 2022**

## **Scientific Amendment**

**I certify that the thesis entitled " *Synthesis of Some Ternary Metal Oxides and sulphides Nanostructures Thin Films for Photovoltaic Applications* " presented by student (Layth Ali Saleh) has been evaluated scientifically, therefore, it is suitable for debate by examining committee.**

**Signature**

**Name: Dr. Isam M. Ibrahim**

**Title: Professor**

**Address: University of Baghdad, College of science, department of Physics**

**Data:     /     / 2022**

## **Linguistic Amendment**

**I certify that the thesis entitled " *Synthesis of Some Ternary Metal Oxides and sulphides Nanostructures Thin Films for Photovoltaic Applications* " presented by (Layth Ali Saleh) has been corrected linguistically; therefore, it is suitable for debate by examining committee.**

**Signature**

**Name: Esam H. Hameed**

**Title: Assistant Professor**

**Address: University of Diyala, College of science**

**Data:    /    / 2022**

## Examination Committee Certificate

We certify that we have read this thesis entitled " *Synthesis of Some Ternary Metal Oxides and sulphides Nanostructures Thin Films for Photovoltaic Applications* " and, as an examining committee, we examined the student (Layth Ali Saleh) on its content, and in what is related to it, and that in our opinion it meets the standard of a thesis for the degree of *Doctor of Philosophy of Science in Physics*.

### (Chairman)

Signature

Name: **Dr. Tahseen H. Mubarak**

Title: Professor

Address: College of Science, University of Diyala

Date:    /    / 2022

### (Member)

Signature

Name: **Dr. Nabeel A. Bakr**

Title: Professor

Address: College of Science,  
University of Diyala

Date:    /    / 2022

### (Member)

Signature

Name: **Dr. Suad.H. Aleabi**

Title: Professor

Address: College of Education (Ibn Al-  
Haitham), University of Baghdad

Date:    /    / 2022

### (Member)

Signature

Name: **Dr. Muslim A . Abid**

Title: Assistant Professor

Address: College of Science,  
Al-Mustansiriyah University

Date:    /    / 2022

### (Member)

Signature

Name: **Dr. Jasim M. Mansoor**

Title: Assistant Professor

Address: College of Science,  
University of Diyala

Date:    /    / 2022

### **(Member / supervisor)**

Signature

Name: **Dr. Ziad Tariq Khodair**

Title: professor

Address: College of Science,  
University of Diyala

Date:    /    / 2022

Approved by the Council of the College of Science

**(The dean)**                      Signature:

Name: **Dr. Tahseen H. Mubarak**

Date:    /    / 2022

Title: professor

# *Dedications*

To

The first teacher who gave me the strength and patience and diligence.

*(My father)*

To

My way candle that lit up my life and stayed up nights to my care.

*(My late Mother)*

*To:*

*The lights of my life*

*My wife and my children*

*To:*

*The lights of my eyes*

*Brothers and sisters*

*To:*

*My beloved country Iraq*

*The martyrs of Iraq with all the love and appreciation*



# *Acknowledgments*

First of all, I would like to thank *Allah*, for his generosity and mercy in giving the strength and the ability to complete my studies.

I would like to express my deep gratitude and appreciation to my supervisor **Prof. Dr. Ziad Tariq Khodair** for suggesting the topic of the thesis and for his continuous advice and guidance during this work.

I would like to express my profound gratitude to **prof. Dr. Nabeel Ali Bakr** for his kind cooperation and constant support and **Prof. Dr. Sabah Anwer Salman**, for his constant encouragement throughout my studies for helping me. study in the Department of Physics, College of Science, University of Diyala.

Special thanks are extended to the University of Diyala, College of Science, Special thanks to the Dean of the College of Science, University of Diyala **Prof. Dr. Tahseen H. Mubarak** and the head of the Physics Department, **Assist .Prof. Dr. Ammar A. Habeeb** and all the Staff of the Department of Physics for their assistance.

Finally, I thank all my classmates and I wish them success and I would also express my deep sense of gratitude to **Omar Ahmad, Shahlaa Munther and Marwa Rashid.**

## Abstract

In this study, thin films of prepared materials ( $\text{Cd}_2\text{SnO}_4$  and  $\text{Zn}_2\text{SnO}_4$ ) were deposited via spray pyrolysis at temperatures (450, 500, and 550 °C), while thin films of prepared materials ( $\text{Cu}_2\text{SnS}_3$  and  $\text{CuZnS}$ ) were deposited using spin coating at temperatures (2000, 250, and 300 °C). The materials NPs ( $\text{Cd}_2\text{SnO}_4$  and  $\text{Zn}_2\text{SnO}_4$ ) were prepared at temperatures of (550 °C) while the materials ( $\text{Cu}_2\text{SnS}_3$  and  $\text{CuZnS}$ ) were prepared at temperatures of (300 °C) using the autocombostion sol-gel method.

The structural, optical, and electrical (Hall effect) properties of the obtained thin films were investigated. X-ray diffraction (XRD) results demonstrated that the films prepared by spray pyrolysis method  $\text{Cd}_2\text{SnO}_4$  and  $\text{Zn}_2\text{SnO}_4$  are polycrystalline with a cubic structure (Spinel), whereas the films prepared by spin coating  $\text{Cu}_2\text{SnS}_3$  are polycrystalline with a tetragonal structure and a hexagonal structure of  $\text{CuZnS}$ , and that an increase in substrate temperature increased the crystal size. Using the Scherer formula, the crystal sizes of ( $\text{Cd}_2\text{SnO}_4$ ,  $\text{Zn}_2\text{SnO}_4$ ,  $\text{Cu}_2\text{SnS}_3$ , and  $\text{CuZnS}$ ) were determined to be 43.8 nm, 22.0 nm, 22.5 nm, and 37.2 nm, respectively. The X-ray diffraction results further revealed that all sol-gel-prepared films of  $\text{Cd}_2\text{SnO}_4$ ,  $\text{Zn}_2\text{SnO}_4$ ,  $\text{Cu}_2\text{SnS}_3$ , and  $\text{CuZnS}$  are polycrystalline with a cubic structure. The FTIR spectra indicated the formation of the materials and the presence of broad vibration peaks (O-H) via spray pyrolysis and spin coating methods.

The existence of nanostructures in the thin films prepared with (XRD, AFM and FE-SEM) techniques was confirmed as the results of atomic force

microscopy (AFM) measurements demonstrated a clear temperature dependence in the values of grain size, surface roughness, and the square root of the mean roughness with the substrate. Through the use of thermal evaporation and spin coating methods. The optical characteristics were investigated by recording the spectrum absorbance and transmittance over a range of wavelengths (300-900 nm).

Thin films of  $\text{Cd}_2\text{SnO}_4$  and  $\text{Zn}_2\text{SnO}_4$  demonstrated a decrease in absorption with rising transmittance values and an increase in wavelength. The results also demonstrated an increase in the values of the absorption coefficient with an increase in the substrate temperature, an increase in the absorption of the films with a decrease in the transmittance values, and an increase in the wavelength of  $\text{Cu}_2\text{SnS}_3$  and  $\text{CuZnS}$ . For the films prepared by spin coating method. It showed that the energy gap values increase with the increase in the substrate temperature of the films prepared by spray pyrolysis method  $\text{Cd}_2\text{SnO}_4$  and  $\text{Zn}_2\text{SnO}_4$  their energy gap values were 2.75 eV and 3.30 eV at 550 °C, respectively. The energy gap of each of  $\text{Cu}_2\text{SnS}_3$  and  $\text{CuZnS}$  was also measured, and it was found to be equal to eV1.65 and eV1.80, respectively, at a temperature of 300 °C, which was prepared by spin coating method.

The Hall effect results demonstrated that increasing the substrate temperature improves the electrical properties of all films, with  $\text{Cu}_2\text{SnS}_3$  having the highest electrical conductivity at  $1.001 \times 10^6 (\Omega \cdot \text{cm})^{-1}$ , which was offset by an increase in the concentration of charge carriers of  $1.23 \times 10^{23} (\text{cm})^{-3}$  and a decrease in electrical resistivity of  $9.987 \times 10^{-7} (\Omega \cdot \text{cm})$ .

$\text{Cd}_2\text{SnO}_4$  and  $\text{Zn}_2\text{SnO}_4$  were subsequently deposited on porous silicon by the spray pyrolysis method, while  $\text{Cu}_2\text{SnS}_3$  and  $\text{CuZnS}$  were deposited via the spin coating method. And  $\text{Cd}_2\text{SnO}_4$ ,  $\text{Zn}_2\text{SnO}_4$ ,  $\text{Cu}_2\text{SnS}_3$ , and  $\text{CuZnS}$  were deposited using the drop-casting method (1 $\mu\text{m}$  thick porous silicon). Then, using spray pyrolysis, aluminum was deposited as a conducting electrode on the back face of the silicon cell. The features of the solar cell and photodetector were

subsequently evaluated. The parameters of the photovoltaic current density (I-V) curves of manufactured solar cells were measured under  $100\text{mW/m}^2$  of simulated solar light. The parameters (open-circuit voltage  $V_{OC}$ ), (closed-circuit current  $I_{SC}$ ), (fill factor FF %), and (solar cell efficiency  $\eta$  %) were determined.

The thin films that were deposited by spin coating method offered the maximum performance, and its value was (4.7%). For heterogeneous junctions (CuZnS)/PSi/n-Si/Al, and the results indicated that the drop-casting approach had a major role in enhancing the performance of the solar cell. The heterojunctions ( $\text{Cu}_2\text{SnS}_3$ )/PSi/n-Si/Al produced the greatest efficiency value (7.80 %). The spectral response measurements of the prepared photodetectors revealed that they performed within the range of (400-900) nm, which is the maximum spectral response value for heterogeneous junction (CuZnS) PSi / n-Si / Al that can be employed for near-infrared photodetector applications. The red and visible spectrum, where the spectral response ( $R\lambda$ ) and specificity detection ( $D^*$ ) of CuZnS/PSi/n-Si/Al photodetectors are approximately (0.60A/W) and ( $9.2 \times 10^{12} \text{ cm Hz}^{1/2} \text{ W}^{-1}$ ) at  $\lambda \sim 450 \text{ nm}$ , respectively.

# Table of Contents

Subject	Page No.
Table of Contents	I
List of Figures	VI
List of Tables	XII
List of Symbol	XIII
List of Abbreviation	XIV

Item No.	Subject	Page No.
<b><i>Chapter One: Overview of Nanomaterials and Literature Review</i></b>		
1.1	Introduction	1
1.2	Thin Films Preparation Methods	2
1.3	Chemical Spray Pyrolysis	3
1.4	Spin Coating Technique	4
1.5	Cadmium Stannate ( $Cd_2SnO_4$ ) Properties	5
1.6	Zinc Stannate ( $Zn_2SnO_4$ ) properties	6
1.7	Copper-Tin-Sulphide ( $Cu_2SnS_3$ ) Properties	7
1.8	Copper-Zinc Sulphide ( $CuZnS$ ) Properties	8
1.9	Literature Review	8-16
1.10	Aim of the work	17

<i>Chapter Two: Theoretical Part</i>		
2.1	Introduction	18
2.2	Nanomaterial	18
2.2.1	Classification of Nanomaterials	18-19
2.3	Quantum Confinement Effect	20
2.4	The Semiconductor Materials	21
2.4.1	Inorganic Semiconductors	22
2.4.2	Organic Semiconductors	22
2.5	Hybrid Organic–Inorganic Semiconductors	23
2.6	Porosity of Porous Silicon	23
2.7	Physical Properties of Thin Films	24
2.7.1	Structural Properties	24
2.8	Atomic Force Microscopy (AFM) Measurements	28
2.9	Field Emission Scanning Electron Microscopy (FE-SEM)	29
2.10	Optical Properties of Crystalline Semiconductors	31
2.10.1	Transmittance (T)	31
2.10.2	Reflectance (R)	31
2.10.3	Absorbance (A)	32
2.11	The Fundamental Absorption Edge	33
2.12	Absorption Regions	33
2.13	The Electronic Transitions	35
2.13.1	Direct Transitions	35
2.13.2	Indirect Transitions	36
2.14	Optical Energy Gap ( $E_g$ )	37
2.15	Optical Constants	38
2.15.1	Absorption Coefficient ( $\alpha$ )	38
2.15.2	FTIR spectra	38
2.16	Electrical Properties	39
2.16.1	Hall Effect	39
2.17	Heterojunctions	42
2.17.1	Abrupt Anisotype Heterojunctions	42
2.18	Electrical Properties of Heterojunction	47
2.18.1	(I-V) Characteristics of Heterojunction	47
2.18.1.1	(I-V) Properties of Heterojunction in the Dark Condition	47
2.18.1.2	Characteristics of Heterojunction (I–V) Under Illumination	50
2.19	Solar cell	51
2.19.1	Photovoltaic (PV)	53
2.20	Generations of Solar Cells	55-56

2.21	Solar Cells Characterizations	56
2.21.1	Short Circuit Current (ISC)	57
2.21.2	Short Circuit Current Density (JSC)	57
2.21.3	Open-Circuit Voltage (VOC)	58
2.21.4	Maximum Voltage (V <sub>max</sub> )	58
2.21.5	Maximum Current (I <sub>max</sub> )	59
2.21.6	Maximum Power (p <sub>max</sub> )	59
2.21.7	Fill Factor (F.F)	59
2.21.8	Power Conversion Efficiency ( $\eta$ )	60
2.22	The Equivalent Electrical Circuit of Solar Cell	60
2.23	Photodetectors	62
2.23.1	Thermal detector	62
2.23.2	Photon Detectors	63
2.24	Photodetector parameters	65
2.24.1	Spectral response measurements	65
2.24.2	Photocurrent Gain (G)	65
2.24.3	Specific Detectivity (D)	66
<b><i>Chapter Three: Experimental Part</i></b>		
3.1	Introduction	67
3.2	Raw Materials	67
3.3	Samples Preparation	69
3.3.1	Preparation of Solution	69
3.3.2	Substrate Preparation	72
3.3.3	Fabrication of Porous Silicon	73
3.3.3.1	Electrodes Deposition	73
3.3.3.2	The Electrochemical Etching Process	73
3.3.3.3	The Photo electrochemical Etching (PEC) Process	74
3.4	Thin Film Deposition	75
3.5	Chemical Spray Pyrolysis System	75
3.5.1	Atomizer	75
3.5.2	Electric heater	76
3.5.3	thermocouple	76
3.6	The Effective Coefficients on the Films Homogeneity	77
3.6.1	Substrate Temperature	77
3.6.2	Substrate Position	77
3.6.3	Vertical Distance	77
3.6.4	Spraying Rate	77
3.6.5	Spraying Time	78
3.6.6	Gas Pressure	78
3.6.7	Deposition Process	78
3.7	Spin Coating Technique	79

3.7.1	Factors that Influence Thin Film Preparation	80
3.7.2	Thin Films Deposition	80
3.7.3	Synthesis of Cd <sub>2</sub> SnO <sub>4</sub> , Zn <sub>2</sub> SnO <sub>4</sub> , Cu <sub>2</sub> SnS <sub>3</sub> and CuZnS nanoparticles by Sol-Gel procedure	81
3.7.3.1	Calculating weight of materials	82
3.7.3.2	Preparation of Cd <sub>2</sub> SnO <sub>4</sub> , Zn <sub>2</sub> SnO <sub>4</sub> , Cu <sub>2</sub> SnS <sub>3</sub> and CuZnS nanoparticles by sol-gel method	83
3.7.3.3	Thin Film Deposition	85
3.8	Preparation of Contact Electrodes	85
3.9	Heat treatment of Samples	86
3.10	Masks Preparation	86
3.11	Device Fabrication	87
3.11.1	Fabrication of heterojunctions (solar cell and photodetectors)	87
3.12	Measurements	88
3.12.1	The Thickness of the thin film	88
3.13	Characterization Techniques	89
3.13.1	Structural Measurement (X-Ray Diffraction)	89
3.13.2	(FE-SEM)	90
3.13.3	Atomic Force Microscope (AFM)	90
3.13.4	Fourier Transform Infrared Spectroscopy (FTIR)	90
3.13.5	UV-Vis Spectroscopy	91
3.13.6	Hall Effect Measurements	91
3.14	Solar Cell Parameters	93
3.14.1	Open-Circuit Voltage Measurement	93
3.14.2	Short-Circuit Current Measurement	93
3.15	Electrical Properties of Heterojunction	93
3.15.1	(I-V) Characteristics Measurement in the Dark Condition	93
3.15.2	(Current-Voltage) Characteristics Measurement under Illumination	94
3.16	Photodetector Properties Measurements	95
3.16.1	Spectral responsivity ( $R_{\lambda}$ )	95
3.16.2	Spectral Detectivity ( $D^*$ )	95
<b><i>Chapter Four: Results and Discussion</i></b>		
4.1	Introduction	96
4.2	Structural Measurements	96
4.2.1	XRD Analysis of (Cd <sub>2</sub> SnO <sub>4</sub> ) Thin films prepared by spray pyrolysis technique	96
4.2.2	XRD Analysis of (Zn <sub>2</sub> SnO <sub>4</sub> ) Thin films prepared by spray pyrolysis technique	98



4.2.3	XRD Analysis of (Cu <sub>2</sub> SnS <sub>3</sub> ) Thin films prepared by spin coating technique	101
4.2.4	XRD Analysis of (CuZnS) Thin films prepared by spin coating technique	103
4.2.5	XRD Analysis of Cd <sub>2</sub> SnO <sub>4</sub> Thin film prepared by drop casting technique	105
4.2.6	XRD Analysis of Zn <sub>2</sub> SnO <sub>4</sub> Thin film prepared by drop casting technique	106
4.2.7	XRD Analysis of Cu <sub>2</sub> SnS <sub>3</sub> Thin film prepared by drop casting technique	108
4.2.8	XRD Analysis of (CuZnS) Thin film prepared by drop casting technique	110
4.2.9	The XRD crystallite size (D)	112
4.2.10	Dislocation Density ( $\delta$ )	116
4.2.11	The Number of crystallites (No)	116
4.3	Fourier Transform Infrared Spectroscopy (FTIR)	117
4.4	Morphological Analysis	122
4.4.1	Atomic Force Microscopy (AFM)	122
4.4.2	Field Emission-Scanning Electron Microscopy (FE-SEM)	128
4.5	Optical Properties of Thin Films	136
4.5.1	Absorbance (A)	136
4.5.2	Transmittance (T)	139
4.5.3	Absorption Coefficient ( $\alpha$ )	142
4.5.4	Optical Energy Gap (E <sub>g</sub> )	144
4.6	Hall effect	148
4.7	Properties of (Cd <sub>2</sub> SnO <sub>4</sub> , Zn <sub>2</sub> SnO <sub>4</sub> , Cu <sub>2</sub> SnS <sub>3</sub> and CuZnS)/PSi Solar Cell by spray pyrolysis and spin coating technique	149
4.7.1	(I-V) Characteristics of Heterojunction in the Dark Condition	150
4.7.2	(I-V) Characteristics Under Illumination (Photocurrent)	153
4.7.3	Short Circuit Current (I <sub>sc</sub> ) and Open Circuit Voltage (V <sub>oc</sub> ) Measurements	155
4.8	Detector Performance Parameters Measurement	161
4.8.1	Spectral Responsivity (R <sub><math>\lambda</math></sub> )	161
4.8.2	Photocurrent Gain (G)	164
4.8.3	Specific Detectivity (D*)	167

## List of Figures

Fig No.	Figure Caption	Page No.
1.1	Various nanostructured thin film synthesis techniques	3
1.2	Crystalline structures of $\text{Cd}_2\text{SnO}_4$ (Cubic spinel)	6
1.3	The cubic spinel structure for $\text{Zn}_2\text{SnO}_4$	6
1.4	Crystallographic structures of $\text{Cu}_2\text{SnS}_3$ (a) Monoclinic, (b) Cubic, (c) Wurtzite, (d) Tetragonal and (e) Hexagonal	7
2.1	Schematic illustration classification of nanomaterials (1) 0D spheres and clusters, (2) 1D Nano fibers, Wires, and Rods (3) 2D Films, Plates, and Networks, (4) 3D Nanomaterials	19
2.2	Schematic of the quantum confinement impact on the energy level structure of a semiconductor material	21
2.3	Interference between waves diffracted from two adjacent rows of atoms in a crystal	25
2.4	(XRD) of (a): Amorphous material (b): Single material, and (c): Polycrystalline material	25
2.5	Schematic of the cantilever-tip assembly used in an AFM	29
2.6	A schematic diagram of the FE-SEM parts	30
2.7	The crystal semiconductor's fundamental absorption edge	33
2.8	The absorption regions in semiconductors	34
2.9	The transition types (a) allowed direct transition (c) allowed indirect transition (b) forbidden direct transition (d) forbidden indirect transition.	37
2.10	Hall Effect measurement setup for electrons	41
2.11	Schematic representation of the tunneling model based on an energy band diagram of Anderson	43
2.12	Typical experimentally observed $\log I$ vs, applied voltage, $V$ , for a p-n heterojunction at three different temperature	45
2.13	Schematic representation of the tunneling-recombination	45

	process	
2.14	Energy band diagram for an abrupt p-n heterojunction, under reverse bias, indicating tunneling mechanism	46
2.15	Semi logarithmic current-voltage characteristics for an abrupt <i>p-n</i> heterojunction	46
2.16	Current-voltage characteristics of an ideal anisotype heterojunction in the dark and under illumination	48
2.17	(I-V) characteristics of a p-n junction diode	50
2.18	p-n junction of solar cell	52
2.19	Structure of a PV cell	54
2.20	Schematic of a solar cell	55
2.21	Typical current density-voltage characteristic of solar cell	57
2.22	Equivalent circuit for a solar cell	61
2.23	Effect of (a) increasing series and (b) reducing parallel resistances	61
2.24	Relative spectral responsivities of perfect detectors	63
3.1	The schematic diagram of the experimental work	70
3.2	Steps of preparing a solution ( $\text{Cu}_2\text{SnS}_3$ and $\text{CuZnS}$ )	72
3.3	Schematic diagram of the electrochemical etching utilized in the study	74
3.4	schematic diagram of PEC system	75
3.5	Spray pyrolysis deposition equipment	79
3.6	a) A photograph of the spin coater instrument used and (b) spin coating stages on the substrat	80
3.7	The diagram of the sol-gel method	82
3.8	The sol-gel steps technique for $\text{Cu}_2\text{SnS}_3$ thin film: (a) solution, (b) gel and (c) burn	84
3.9	The sol-gel steps technique for $\text{Zn}_2\text{SnO}_4$ thin film: (a) solution, (b) gel and (c) burn	85
3.10	Schematic diagram drop casting method experimental setup	86
3.11	Mask for Hall effect	86
3.12	The basic structure of typical ( $\text{Cd}_2\text{SnO}_4$ , $\text{Zn}_2\text{SnO}_4$ , $\text{Cu}_2\text{SnS}_3$ and $\text{CuZnS}$ )/PSi/Si/Al heterojunction	87
3.13	Porous silicon membrane	88

3.17	Fourier transform infrared spectroscopy system	90
3.18	UV-Vis system	91
3.19	Hall effect Measurement system	92
3.20	(a) image of the sample base on which the samples are placed (b) image of the prepared samples	92
3.21	Ideal Circuit diagram used to measure current-voltage characteristics in the dark case	94
3.22	The system was used to measure the spectral response of the prepared photovoltaic detectors	95
4.1	X-ray Diffraction of $\text{Cd}_2\text{SnO}_4$ thin films deposited at different substrate temperatures (450, 500 and 550 °C) prepared by spray pyrolysis	97
4.2	X-ray Diffraction of $\text{Zn}_2\text{SnO}_4$ thin films at different substrate temperatures (450, 500 and 550 °C) prepared by spray pyrolysis	99
4.3	X-ray Diffraction of $\text{Cu}_2\text{SnS}_3$ thin films at different substrate temperatures (200, 250 and 300 °C) deposited and annealed	102
4.4	X-ray Diffraction of $\text{CuZnS}$ thin films at different substrate temperatures (200, 250 and 300 °C) deposited and annealed	104
4.5	X-ray Diffraction of $\text{Cd}_2\text{SnO}_4$ thin films prepared by the drop-casting method that annealed at temperature (550 °C)	105
4.6	X-ray Diffraction of $\text{Zn}_2\text{SnO}_4$ thin films prepared by drop-casting method that annealed at temperature (550 °C)	107
4.7	X-ray Diffraction of $\text{Cu}_2\text{SnS}_3$ thin films prepared by drop-casting method that annealed at a temperature (300 °C)	109
4.8	X-ray Diffraction of $\text{CuZnS}$ thin films prepared by drop-casting method that annealed at a temperature (300 °C)	111
4.9	The W-H analysis of $\text{Cd}_2\text{SnO}_4$ and $\text{Zn}_2\text{SnO}_4$ thin films at different substrate temperature (450, 500 and 550°C)	113--114
4.10	The W-H analysis of $\text{Cu}_2\text{SnS}_3$ and $\text{CuZnS}$ thin films that were deposited on glass substrate and annealed at different substrate temperatures (200, 250 and 300 °C) prepared by spin coating method	115
4.11	FTIR transmittance spectra of $\text{Cd}_2\text{SnO}_4$ thin film that was deposited on glass substrate at different substrate temperatures (450, 500 and 550°C) prepared spray pyrolysis method	118
4.12	FTIR transmittance spectra of $\text{Zn}_2\text{SnO}_4$ thin film that was deposited on glass substrate at different substrate	119

	temperatures (450, 500 and 550 °C) prepared by spray by pyrolysis method	
4.13	FTIR transmittance spectra of Cu <sub>2</sub> SnS <sub>3</sub> thin film deposited on glass substrate and annealed at different temperatures (200, 250 and 300 °C) prepared by spin coating method	120
4.14	FTIR transmittance spectra of CuZnS thin film deposited on glass substrate and annealed at different temperatures (200, 250 and 300 °C) prepared by spin coating method	121
4.15	3-D AFM images for thin (Cd <sub>2</sub> SnO <sub>4</sub> , Zn <sub>2</sub> SnO <sub>4</sub> , Cu <sub>2</sub> SnS <sub>3</sub> and CuZnS) thin films deposited at different substrate temperature	124-125
4.16	Granularity accumulation distribution charts for (Cd <sub>2</sub> SnO <sub>4</sub> , Zn <sub>2</sub> SnO <sub>4</sub> , Cu <sub>2</sub> SnS <sub>3</sub> and CuZnS) thin films deposited at different substrate temperature	126-127
4.17a	FE- SEM picture for Cd <sub>2</sub> SnO <sub>4</sub> with ( cross-section) and planner Volumetric distribution	130-131
4.17b	FE-SEM picture for Zn <sub>2</sub> SnO <sub>4</sub> with (cross-section) and planner Volumetric distribution	131-132
4.17c	FE- SEM picture for Cu <sub>2</sub> SnS <sub>3</sub> with ( cross-section) and planner Volumetric distribution	133-134
4.17d	FE-SEM picture for CuZnS with and planner Volumetric distribution	134-135
4.18a	The absorbance of Cd <sub>2</sub> SnO <sub>4</sub> thin films wear deposited prepared by spray pyrolysis method at different substrates temperatures (450, 500 and 550 °C)	137
4.18b	The absorbance for Zn <sub>2</sub> SnO <sub>4</sub> thin films at different substrates temperature (450,500 and 550 °C)	137
4.18c	The absorbance of Cu <sub>2</sub> SnS <sub>3</sub> thin films wear deposited and annealed prepared by spin coating method at different substrates temperatures (200, 250 and 300 °C)	138
4.18d	The absorbance of CuZnS thin films wear deposited and annealed prepared by spin coating method at different substrates temperatures (200, 250 and 300 °C)	138
4.19a	The transmittance spectrum for deposited (Cd <sub>2</sub> SnO <sub>4</sub> ) thin film as a function of wavelength at different substrate temperature (450, 500 and 550°C)	140
4.19b	The transmittance spectrum for deposited (Zn <sub>2</sub> SnO <sub>4</sub> ) thin film as a function of wavelength at different substrate temperature (450,500 and 550°C)	140
4.19c	The transmittance spectrum for deposited (Cu <sub>2</sub> SnS <sub>3</sub> ) thin film as a function of wavelength at different substrate temperature (200, 250 and 300°C)	141

4.19d	The transmittance spectrum for deposited (CuZnS) thin film as a function of wavelength at different substrate temperature (200, 250 and 300°C)	141
4.20a	The absorption coefficient for deposited Cd <sub>2</sub> SnO <sub>4</sub> thin film as a function of wavelength at different substrate temperature (450, 500 and 550°C)	142
4.20b	The absorption coefficient for deposited Zn <sub>2</sub> SnO <sub>4</sub> thin film as a function of wavelength at different substrate temperature (450, 500 and 550°C)	143
4.20c	The absorption coefficient for deposited Cu <sub>2</sub> SnS <sub>3</sub> thin film as a function of wavelength at different substrate temperature (200, 250 and 300°C)	143
4.20d	The absorption coefficient for deposited CZS thin film as a function of wavelength at different substrate temperature (200, 250 and 300 °C )	144
4.21a	( $\alpha h\nu$ ) <sup>2</sup> as a function of photon energy for Cd <sub>2</sub> SnO <sub>4</sub> films prepared at different substrates temperatures a (450, 500 and 550°C)	145
4.21b	( $\alpha h\nu$ ) <sup>2</sup> as a function of photon energy for Zn <sub>2</sub> SnO <sub>4</sub> films prepared at different substrates temperatures a (450, 500 and 550°C)	146
4.21c	( $\alpha h\nu$ ) <sup>2</sup> as function of energy photon for nanostructure Cu <sub>2</sub> SnS <sub>3</sub> thin films deposited at different substrate temperature (200,250 and 300°C)	146
4.21d	( $\alpha h\nu$ ) <sup>2</sup> as function of energy photon for nanostructure CuZnS thin films deposited at different substrate temperature (200,250 and 300 °C)	147
4.22	I-V characteristics in the dark for both reverse and forward bias of Cd <sub>2</sub> SnO <sub>4</sub> /PSi / p-Si/Al	151
4.23	I-V characteristics in the dark for both reverse and forward bias of Zn <sub>2</sub> SnO <sub>4</sub> /PSi/p-Si/Al	151
4.24	I-V Characteristics in the dark for both reverse and forward bias of Cu <sub>2</sub> SnS <sub>3</sub> /PSi /n-Si/ Al at 300°C	152
4.25	I-V characteristics in the dark for both reverse and forward bias of CuZnS/PSi /n-Si/Al	152
4.26	I-V characteristics in the dark and under light in the case of reverse bias of Cd <sub>2</sub> SnO <sub>4</sub> /PSi/p-Si/ Al	153
4.27	I-V Characteristics in the dark and under a light in the case of reverse bias of Zn <sub>2</sub> SnO <sub>4</sub> /PSi/p-Si/ Al	154
4.28	I-V characteristics in the dark and under light in the case of reverse bias of Cu <sub>2</sub> SnS <sub>3</sub> /PSi/n-Si/ Al	154

4.29	I-V characteristics in the dark and under light in the case of reverse bias of CuZnS/ PSi/n-Si/ Al	155
4.30	I-V Curve of a solar cell (SC) of Cd <sub>2</sub> SnO <sub>4</sub> /PSi/p-Si/Al	156
4.31	I-V Curve of a solar cell (SC) of Zn <sub>2</sub> SnO <sub>4</sub> /PSi/p-Si/ Al	156
4.32	I-V Curve of a solar cell (SC) of Cu <sub>2</sub> SnS <sub>3</sub> /PSi/n-Si/Al	157
4.33	I-V Curve of a solar cell (SC) of CuZnS/PSi/n-Si/Al	157
4.34	I-V Curve of a solar cell (SC) of Cd <sub>2</sub> SnO <sub>4</sub> /PSi/p -Si/Al	159
4.35	I-V Curve of a solar cell (SC) of Zn <sub>2</sub> SnO <sub>4</sub> / PSi/p -Si/ Al	159
4.36	(I-V) curve of solar cell (SC) of Cu <sub>2</sub> SnS <sub>3</sub> / PSi/n-Si/Al	160
4.37	(I-V) curve of solar cell (SC) of CuZnS/ PSi/n-Si/Al	160
4.38	The variation of spectral responsivity with wavelength for Cd <sub>2</sub> SnO <sub>4</sub> /p-PSi/Al	162
4.39	The variation of spectral responsivity with wavelength for Zn <sub>2</sub> SnO <sub>4</sub> /p-PSi /Si/ Al	163
4.40	The variation of spectral responsivity with wavelength for Cu <sub>2</sub> SnS <sub>3</sub> / PSi /n-Si/Al	163
4.41	The variation of spectral responsivity with wavelength for and CuZnS / PSi/n-Si/Al	164
4.42	The variation of photocurrent Gain (G) with wavelength for Cd <sub>2</sub> SnO <sub>4</sub> / PSi/p-Si/Al	165
4.43	The variation of photocurrent Gain (G) with wavelength for Zn <sub>2</sub> SnO <sub>4</sub> /PSi/p-Si/Al	165
4.44	The variation of photocurrent Gain (G) with wavelength for Cu <sub>2</sub> SnS <sub>3</sub> /PSi/n-Si/Al	166
4.45	The variation of photocurrent Gain (G) with wavelength for CuZnS/PSi/n-Si/Al	166
4.46	The variation of spectral detectivity with wavelength for Cd <sub>2</sub> SnO <sub>4</sub> /PSi /p-Si/Al	168
4.47	The variation of spectral detectivity with wavelength for Zn <sub>2</sub> SnO <sub>4</sub> /PSi/p-Si/ Al	168
4.48	The variation of spectral detectivity with wavelength for Cu <sub>2</sub> SnS <sub>3</sub> / PSi/n-Si/Al	169
4.49	The variation of spectral detectivity with wavelength for Cu ZnS / PSi/n--Si/Al	169

## List of Tables

Table No.	Table caption	Page No.
2.1	Some inorganic semiconductors	22
2.2	Spectral range of wavelengths of electromagnetic radiation	64
3.1	Raw Materials	67-68
3.2	Masses of materials that make up the thin films (CTO, ZTO, CTS and CZS)	71
3.3	Masses of materials that make up the thin films ( $\text{Cd}_2\text{SnO}_4$ , $\text{Zn}_2\text{SnO}_4$ , $\text{Cu}_2\text{SnS}_3$ and $\text{CuZnS}$ ) by Sol-Gel method	83
4.1	X-ray Diffraction of $\text{Cd}_2\text{SnO}_4$ thin films deposited at different substrate temperatures (450, 500 and 550 °C) prepared by spray pyrolysis	97
4.2	X-ray Diffraction of $\text{Zn}_2\text{SnO}_4$ thin films deposited at different substrate temperatures (450, 500 and 550 °C) prepared by spray pyrolysis	100
4.3	X-ray diffraction results of $\text{Cu}_2\text{SnS}_3$ thin films prepared by spin coating technique	102
4.4	X-ray diffraction results of $\text{CuZnS}$ thin films prepared by spin coating technique	104
4.5	X-ray diffraction results of $\text{Cd}_2\text{SnO}_4$ thin films prepared by drop-casting technique	106
4.6	X-ray diffraction results of $\text{Zn}_2\text{SnO}_4$ thin films prepared by drop-casting technique	108
4.7	X-ray diffraction results of $\text{Cu}_2\text{SnS}_3$ thin films prepared by drop-casting technique	110
4.8	X-ray diffraction results of $\text{CuZnS}$ thin films prepared by drop-casting technique	111
4.9	Structural parameters for ( $\text{Cd}_2\text{SnO}_4$ , $\text{Zn}_2\text{SnO}_4$ , $\text{Cu}_2\text{SnS}_3$ , and $\text{CuZnS}$ ) thin films prepared at different substrate temperatures spray pyrolysis and spin coating	117
4.10	AFM images of surface roughness, root mean square (RMS), and grain size of $\text{Cd}_2\text{SnO}_4$ , $\text{Zn}_2\text{SnO}_4$ , $\text{Cu}_2\text{SnS}_3$ , and $\text{CuZnS}$ thin films at different substrate temperatures	123
4.11	Values of smallest and largest particle size and average particle size of the prepared films $\text{Cd}_2\text{SnO}_4$ , $\text{Zn}_2\text{SnO}_4$ ,	129



	Cu <sub>2</sub> SnS <sub>3</sub> and CuZnS by spray pyrolysis and spin coating	
4.12	Values band gap of Cd <sub>2</sub> SnO <sub>4</sub> , Zn <sub>2</sub> SnO <sub>4</sub> , Cu <sub>2</sub> SnS <sub>3</sub> and CuZnS at different temperature	147
4.13	Hall effect measurement result Cd <sub>2</sub> SnO <sub>4</sub> , Zn <sub>2</sub> SnO <sub>4</sub> , Cu <sub>2</sub> SnS <sub>3</sub> and CuZnS thin films at different substrate temperature	149
4.14	Short-circuit current density, open-circuit voltage, filling factor and efficiency of prepared heterojunctions by spray pyrolysis and spin coating technique	158
4.15	Short-circuit current density, open-circuit voltage, filling factor, and efficiency of prepared heterojunctions by drop-casting technique	161
4.16	Spectral Response, Gain, and Specific Detectivity values for prepared heterojunctions	169

## List of Symbols

Symbol	Meaning	Units
$\lambda$	The wavelength of the incident X- ray	nm
$\theta$	Bragg's angle	degree
$n$	Integer number	-
D	crystallite size	nm
k	Shape factor	-
$a, b \text{ and } c$	Lattice constants	Å
hkl	Miller indices	-
$d_{hkl}$	Inter planar spacing	Å
$\beta$	Full width at half maximum	Degree
$\delta$	Dislocation Density	cm <sup>-2</sup>
$N_o$	Number of crystallites per unit area	cm <sup>-2</sup>
T	Transmittance	-

$I_o$	Incident light intensity	$\text{mW}/\text{cm}^2$
$I_T$	Transmitted light intensity	$\text{mW}/\text{cm}^2$
$R$	Reflection	-
$I_R$	Reflectance light intensity	$\text{mW}/\text{cm}^2$
$n$	Refractive Index	-
$A$	Absorbance	-
$\epsilon$	Micro strain	-
$A'$ and $B$	Constant depending on properties of bands	-
$h$	Planck 's constant	J.s
$h\nu$	Photon energy	eV
$E_g$	Optical Energy Gap	eV
V.B	Valence band	eV
C.B	Conduction Band	eV
$r$	Exponential coefficient depends on the type of transition	-
$\alpha$	Optical absorption coefficient	$\text{cm}^{-1}$
$E_u$	Urbach energy	meV
$\vec{k}$	Wave vector	$\text{cm}^{-1}$
$E_{\text{ph}}$	Phonon energy	eV
$t$	Film Thickness	nm
$R_s$	Series resistance	$\Omega$
$R_{\text{Sh}}$	Shunt resistance	$\Omega$
$\mu_H$	Hall mobility	$\text{m}^2 /(\text{V.s})$
$n_H$	Concentration of charge carriers	$(\text{cm})^{-3}$
$R_H$	Hall coefficient	$\text{m}^3/\text{C}$
$\sigma$	Conductivity	$(\Omega.\text{m})^{-1}$
$V_H$	Hall Voltage	V
$B_z$	magnetic field strength	Tesla
$V$	Voltage	V

$V_a$	Applied Voltage	V
$K_B$	Boltzmann constant	J/K
$q$	Electron charge	C
$I_{ph}$	The light-generated current density	mA
$I_L$	Light induced current	mA
$I_d$	Dark current	mA
$\dot{n}$	The diode ideality factor	-
$T$	Temperature	K
$I_o$	The saturation current density	mA
$I_E$	Electric current	mA
$I_{max}$	Maximum current	mA
$I_{sc}$	Short circuit current	mA
$I_{sh}$	Shunt current	mA
$V_{max}$	Maximum voltage	V
$V_{OC}$	Open-circuit voltage	V
$J_{max}$	Current density at maximum power point	mA/cm <sup>2</sup>
$J_{sc}$	Short- circuit current density	mA/cm <sup>2</sup>
F.F	Fill Factor	-
$\eta$	Efficiency	-
$P_{in}$	The incident power	mW/cm <sup>2</sup>
$P_{max}$	Maximum power	mW/cm <sup>2</sup>
$R_\lambda$	Responsivity	A.W <sup>-1</sup>
$D_\lambda^*$	Spectral Detectivity	cm.Hz <sup>1/2</sup> .W <sup>-1</sup>
$G$	Photocurrent Gain	-
$\mathcal{A}$	The active surface area of the cell	cm <sup>2</sup>

## List of Abbreviations

Abbreviation	Definition
AFM	Atomic Force Microscope
FE-SEM	Field emission scanning electron microscopy
FTIR	Fourier Transform-Infrared Spectroscopy
FWHM	Full Width at Half Maximum
<i>hkl</i>	Miller Indices
I-V	Current-Voltage
J-V	Current density–Voltage
P	Porosity
PCE	Power Conversion Efficiency
PD	Photodetector
PL	Photoluminescence
PSi	Porous Silicon
PV	Photovoltaic
RMS	Root Mean Square
UV	Ultra violet
Vis	Visible
W-H	Williamson-Hall
XRD	X- ray Diffraction

# Chapter One

Overview of Nanomaterials  
and  
Literature Review

## Introduction

When a material's size is lowered to the nanoscale, its chemical and physical characteristics are radically altered. Nanoscience focuses on controlling the formation of nanostructures and morphology, whereas nanotechnology studies the link between matter's size and function [1]. Thin-film physics is a subfield of solid-state physics that will ultimately become a discipline. A layer with a thickness of tens of nanometers is referred to as a nanolayer (film). Thin film has a thickness of less than one micron, according to a published [2]. Because the film layer is so light, it is only placed on the specific type of substrates depending on the study's nature or scientific requirement necessity. Glass slides, silicon wafers, aluminum, quartz, and other substrates are among them. Properties of a thin film vary from bulk material depending on the kind of significant research. Thin films were produced for the first time in 1852 by (Busen & Grove) by a chemical reaction, and a thin metallic film was obtained in 1857 by the scientist (Farady) using thermal evaporation [3]. Furthermore, various factors influence the characteristics of thin films, including the thickness and kind of film utilized, as well as the evaporation conditions employed to make the films. Thin films have a wide range of applications, including rectifiers then junction diodes, integrated circuits, optical communications as light-emitting diodes, semiconductor lasers and detectors, light filters, solar cells, and special-purpose mirrors [4]. In addition, they are used in a range of applications to protect thin-film-painted materials from corrosion, environmental contact, and surface deterioration [5]. The sensitive materials that are convenient for manufacture using a variety of electrical, optical, then optoelectronic possessions are required for a broad area of semiconductor applications. Rather than thinning down bulk material, thin films are generated by depositing ingredients onto a clean, supporting substrate to build up film thickness[6].

## Thin Films Preparation Methods

Thin film properties are quietly sensitive to the preparation method. Different techniques have been developed to deposition thin film on alloys, polymers, superconductors, and metals on several kinds of substrate materials. Indeed, no technique can deposit thin films that cover all the desirable aspects like equipment cost, deposition conditions, substrate material nature, etc. The broad types of thin-film materials, their deposition methods, processing, spectroscopic characterization, fabrication technologies, optical characterization investigations, physical and chemical properties, and structure-property relationships are the main features of these devices and the basis of thin-film technologies. The achievement and economics of thin-film components are the industrialization techniques used to produce the devices. Several techniques are valuable and available to enhance nanostructure thin film in a wide range of potential applications. The production techniques of nanostructured thin film are usually classified into two categories, as shown in figure 1.1:

- (i) Physical techniques, such as the evaporation or sputtering of the material from source and deposition on a substrate, etc. [7].
- (ii) Chemical techniques like a chemical reaction between volatile/non-volatile compounds of the material and deposition on the various substrates etc. [8].

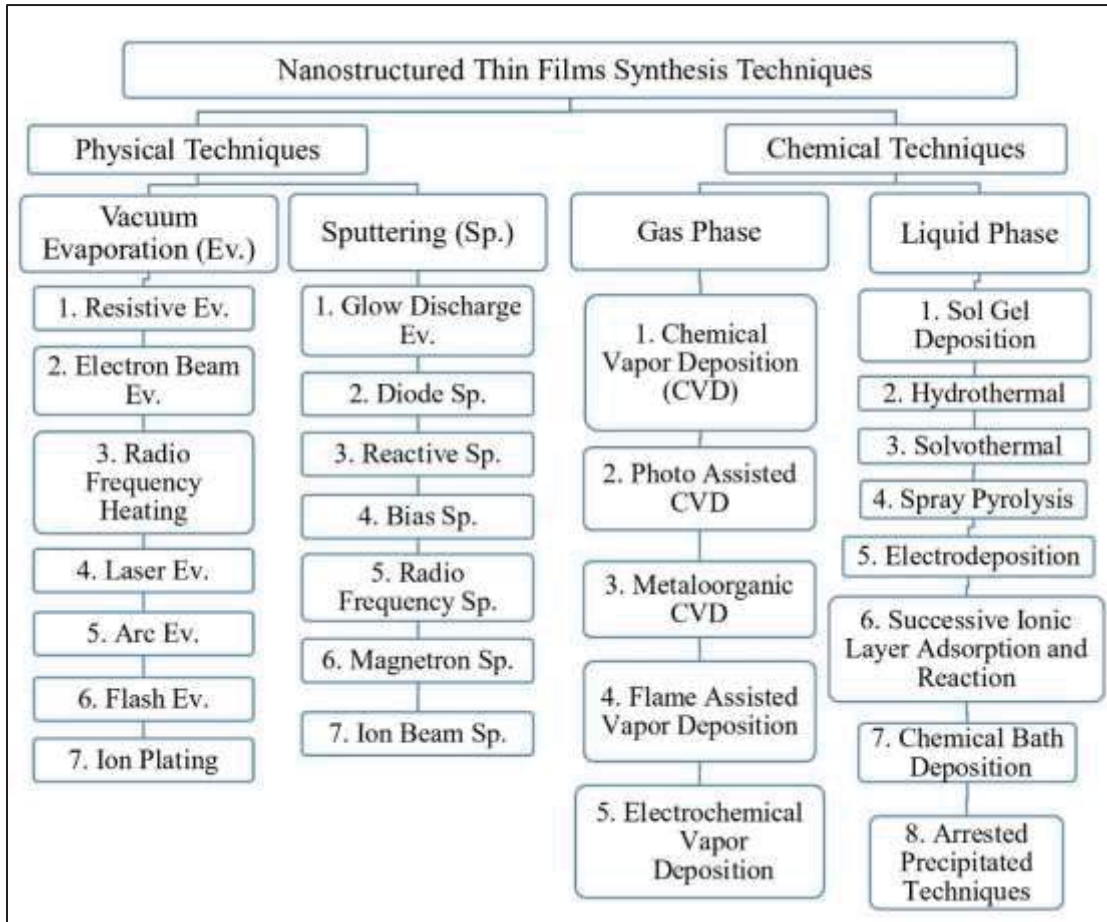


Figure 1.1 Various nanostructured thin film syntheses techniques [9].

### 1.1.1 Spray Pyrolysis Technique

One of the most common processes for generating big area homogeneous coatings is Chemical Pyrolysis by spraying. Chemical Pyrolysis by spraying, is particularly beneficial in the fabrication of conventional and thermal mirrors and very competent filters plus solar cells [10]. One of the most frequent depositings of a wide-ranging of materials in thin-film form. It Chemical Pyrolysis by spraying. For manufacturing high-quality thin films, variables such as substrate temperature, spray rate, and solution concentration, among others, must be fine-tuned. Atomization pyrolysis have on the other hand, get a lot of interest [11]. Spray pyrolysis involves spraying an aqueous solution containing soluble salts of the constituent atoms of the desired compounds to the heated substrates onto a



techniques like ultrasonic nebulization, better Pyrolysis by spraying. Coronas Pyrolysis by spraying., electronic Pyrolysis by spraying., and microprocessor-based spray pyrolysis have on the other hand, get a lot of interest [11]. Particles of the required chemicals are dissolved in water and then sprayed over heated surfaces that are held at high temperatures for spray pyrolysis. This is done in order to break down the compounds in question. When the sprayed droplets reach the hot substrate, they undergo pyrolysis breakdown and produce a single crystal or cluster of crystallites. In the vapor phase, various volatile byproducts and excess solvents escape [12]. Despite its flaws, this approach has numerous advantages [13, 14].

- 1- Safe low-cost and simple technique.
- 2- The necessary equipment cost and raw materials are inexpensive.
- 3 -Using high-quality targets and substrates is not essential.
- 4 -Spray settings can be adjusted to manage film thickness and uniformity.
- 5- It can be used in any type of weather.
- 6- It has the ability to manufacture thin film materials with a high melting point.
- 7- It has the ability to produce thin-film materials with excellent homogeneity and enormous dimensions.

### Spin Coating Technique

A Spin coating is a fast and most commonly utilized chemical deposition method for producing thin and homogenous organic or inorganic sensing from solution. This method enables the creation of very repeatable and homogeneous films. Two forces act on the solution during spin coating: adhesive forces at the solution substrate contact and centrifugal forces induced by the high-speed spinning. These two opposing forces will cause a considerable shearing action at the interface, leading the solution to create a thin film of varying thickness,

determined by rotating velocity, solution concentration, and a viscosity [15]. Several factors must be considered to generate homogeneous films, including solvent evaporation rate, fluid viscosity, solution concentration, angular velocity (rotation speed), and spinning time. The advantage of the spin coating technique is its high ability to provide thin films with thickness ranging from a few nanometers to a few microns in an easy, quick and economical way, the film thickness can be easily changed by changing spin speed, and it is considered a low-cost operating system [16].

### **Cadmium Stannate ( $\text{Cd}_2\text{SnO}_4$ )**

$\text{Cd}_2\text{SnO}_4$  films have a spinel cubic polycrystalline structure as shown in fig 1.2. The cations ratio of Cd and Sn has an essential role in achieving a homogeneous structure of thin-film without any secondary phases, and the lattice parameters have an approximate value of  $a=b=c=0.9174$  nm [17, 18]. Cadmium tin oxide is a n-type semiconductor [17]. It has high carrier mobility, with n-type doping, The visible absorption edge goes to considerably higher energy [19]. Cadmium stannate has a low electrical resistivity, good transmittance in the visible light spectrum, and low reflection in the near IR range. Spray pyrolysis was used to make thin films of  $\text{Cd}_2\text{SnO}_4$  with a 3eV energy bandgap [20].  $\text{Cd}_2\text{SnO}_4$  thin films were demonstrated. It has been several essential advantages of the CdTe/CdS-based solar cells. In contrast, they have the best adhesion to the CdTe/CdS solar cells with respect to tin oxide ( $\text{SnO}_2$ )[21].

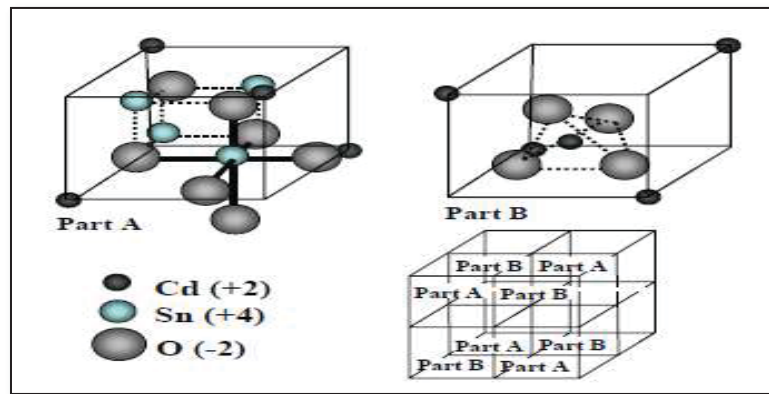


Figure 1.1 Crystalline structures of  $\text{Cd}_2\text{SnO}_4$  (Cubic spinel) [17].

### 1.1.1.1 in Stannate nanosystems

Because of their unique features in optics and electronics, ZnO and  $\text{SnO}_2$  have gotten a lot of attention in recent years. However, ternary semiconductors  $\text{Zn}_2\text{SnO}_4$  may have received better properties and are still less studied and investigated. As it has high-electron mobility, high-electrical conductivity, and significant optical properties, all of these properties make it to be appropriate for solar cell, dye sensitized solar cell, gas sensor Li-ion battery and photodetectors applications [22, 23]. Fig 1.3  $\text{Zn}_2\text{SnO}_4$  has a polycrystalline crystal structure (cubic spinel) [24], with the lattice parameters  $a=b=c= 8.657 \text{ nm}$  [25]. has a lot of electron mobility . Pyrolysis by spraying was used to make thin film. Of high electrical, an n-type transparent conductive oxide with a conductivity of  $3.7 \text{ e V}$  and a large [24].

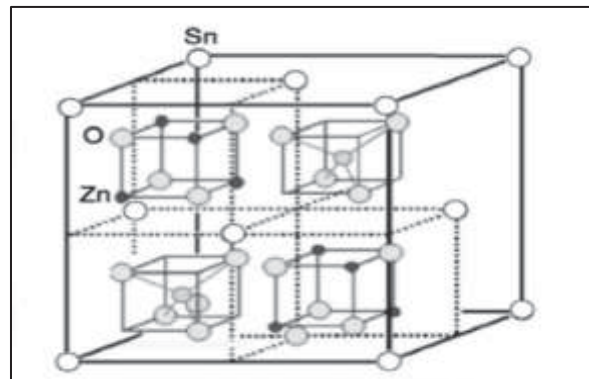


Figure 1.3 The cubic spinel structure of  $\text{Zn}_2\text{SnO}_4$  [24].

## Crystallographic Structures in $\text{Cu}_2\text{SnS}_3$ Compounds

Since 1960, the Cu–Sn–S system has been considered.  $\text{Cu}_2\text{SnS}_3$ ,  $\text{Cu}_3\text{SnS}_4$ , and  $\text{Cu}_4\text{SnS}_4$  are the three phases in this system.  $\text{Cu}_2\text{SnS}_3$  exhibits polymorphs such as monoclinic, cubic, tetragonal, and triclinic as shown in figure 1.4 structures in . Additionally,  $\text{Cu}_2\text{SnS}_3$  crystallizes in wurtzite and hexagonal nanocrystalline form . They've been discovered to be an important absorbent for solar cell use. The (Cu–Sn–S) system is part of the (I–IV–VI) group, and it contains non-toxic, abundant, and inexpensive elements. Due to its usefulness in a wide range of applications, the ternary  $\text{Cu}_2\text{SnS}_3$  (CTS) semiconductor has recently gained a lot of attention. This system's optoelectronic features make it ideal for this application. As photovoltaic devices, the electrical conductivity of the p-type with band gap may be controlled in an optimal range from (1.0 to 1.5 eV). A high optical absorption value of  $\sim 10^5 \text{ cm}^{-1}$  is also seen. CTS thin films have been tried as absorbers solar cells using thin films (TFSCs) by a variety from approaches such as evaporation, sputtering, electro-deposition, pulsed laser deposition and chemical bath deposition [26-28].

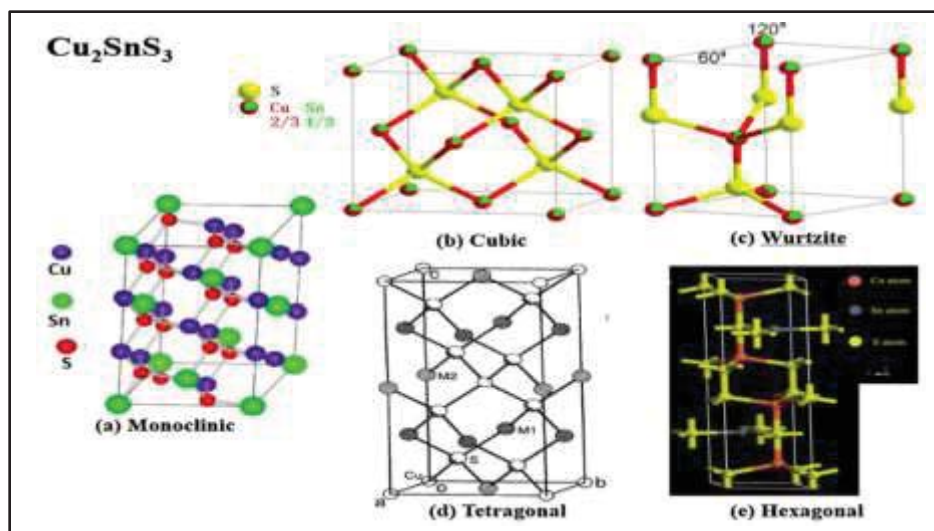


Figure 1.4 Crystallographic structures of  $\text{Cu}_2\text{SnS}_3$  (a) Monoclinic, (b) Cubic, (c) Wurtzite, (d) Tetragonal and (e) Hexagonal [27].

## 2.3.6. CuS thin films

CuS is an essential semiconductor with unique electrical, chemical, and optical characteristics and a wide range of solar cell applications. CuS thin films have recently exposed ability in applications for example gas-sensor materials [29]. 2.36 eV and 2.03 eV it direct bandgap has CuS with a hexagonal structure, according to structural and optical analysis [30]. The most significant rate of all (II–VI) composite semiconductors with n-type semiconductor and broad direct bandgap is (ZnS), which has an energy bandgap of (3.65 eV). It can therefore be utilized in optoelectronics and as an anti-reflective coating for heterojunction solar cells [31].

Nanocomposites thin films' structural, morphological, optical, and electrical properties have recently become an interesting topic due to their unique techniques. CuZnS ternary compounds are a promising nanostructured material for electroluminescent and photoconductor devices, as well as photovoltaic cells. The nano-composite films can also be used as a solar cell absorber. Improvements in the characterisation of copper-zinc sulphide (CZS) are of particular importance since these spectacular p-type inorganic materials have a large direct band gap and are crucial in solar cell applications [29].

## 2.3.7. Literature review

Li et al. [29] Direct liquid coating (DLC) was used to precipitate thin films of tetragonal  $\text{Cu}_2\text{SnS}_3$  (CTS) made of a metal-thiourea compound methanolic precursor solution. X-ray Diffraction confirms the formation of tetragonal  $\text{Cu}_2\text{SnS}_3$ . AFM and scanning electron microscopy demonstrated that the films are soft and uniform with a roughness (RMS) of 1–2 nm energy band gap ( $E_g$ ) for  $\text{Cu}_2\text{SnS}_3$  1.12 eV plus  $10^5 \text{ cm}^{-1}$  for absorption coefficient ( $\alpha$ ), according to optical measurements. The films are p-type, with a  $0.5 \text{ s/cm}$

electrical conductivity(s), rendering to hall measurements, The concentration and mobility of holes are around ( $10^{18} \text{ cm}^{-3}$  and  $1 \text{ cm}^2/\text{V/s}$ ), respectively. DLC developed non-toxic thin-film solar cells (TFSC) made from graphite/ $\text{Cu}_2\text{SnS}_3/\text{ZnO}/\text{ITO}/\text{SLG}$  with a power transformation efficiency PCE of 2.10 % and voltage in the open circuit., current in a short circuit, and the fill factor 0.816 V,  $6.14 \text{ mA}/\text{cm}^2$ , plus 0.42, respectively [32].

**Sreedhar et al** Chemical spray pyrolysis was used to make  $\text{CuZnS}$  thin films. Rendering to the findings, the material may be transformed of n-type to p-type with a 4-order improvement in electrical conductivity by just increasing the Cu content. In comparison, increasing Cu content causes the band-gap to decrease from 3.4 - 1.8 eV. High Cu concentration films are more absorbent, but low Cu concentration films can be employed as a buffer/window layer in solar cells. The absorber layer was  $\text{CuZnS}$ , and the buffer layer was  $\text{In}_2\text{S}_3$ . The J-V possessions from the cell were measured by Ag as the highest electrode.  $V_{oc} = 0.451 \text{ V}$ ,  $J_{sc} = 5.47 \text{ mA}/\text{cm}^2$ ,  $FF = 42.2 \%$ , and  $\eta = 1.04\%$  were the parameters obtained for the optimal doped cell [33].

**oines et al** On glass substrates, the researcher developed  $\text{Cd}_2\text{SnO}_4$  polycrystalline thin films with cubic phase using the sol-gel process. Commencing with a combination of two simple  $\text{CdO}$  and  $\text{SnO}_2$  precursor solutions and thin films formed at room temperature. In the precursor solution, the atomic concentrations of Sn (x) in relation to Cd (1-x) were x=16, 25, 29, 32, 35, and 40. After the annealing operations,  $\text{Cd}_2\text{SnO}_4$  films retained their spinel-type crystalline structure. The Cd/Sn ratio of the  $\text{Cd}_2\text{SnO}_4$  compounds was closest to that of the  $\text{Cd}_2\text{SnO}_4$  compounds at x=29 at % without annealing.  $\text{Cd}_2\text{SnO}_4$  films demonstrated good optical transmission ~85% in the  $500 \text{ nm} < \lambda <$

1500 nm range, both with and without annealing. For  $\text{Cd}_2\text{SnO}_4$  films (x=33 at%) annealed in a vacuum at 550 °C, a minimum resistivity of roughly  $2 \times 10^{-3} \Omega \text{ cm}$  was found, by a direct band gap energy of 3.55 eV [34].

**ao et al** A method for producing high-quality, homogenous, and band-gap-adjustable  $\text{Zn}_2\text{SnO}_4$  nanotubes has been published. By altering the heat treatment temperature, These nanotubes can be autologous-assemble inside a range from different nanofilms by changeable. Gaps in optical bands ranging of 3.54 to 3.18 eV. The  $\text{Zn}_2\text{SnO}_4$  nanotube-nanofilm-based UV-light photo detectors have been successfully produced and show much greater photocurrent and a bigger photocurrent to dark current part than separate nanostructure-founded UV-light photodetectors. Top-showing photo detectors, solar cells, plus Li-ion battery electrode materials could all benefit from it [35].

**anai et al** According to experts,  $\text{Cu}_2\text{SnS}_3$  is a p-type semiconductor that has an coefficient of absorption of over  $10^4 \text{ cm}^{-1}$  and a bandgap energy of 0.92 to 1.77 eV. As a result, it has proven to be a highly absorbent layer to thin-film solar cells. According to this study, CTS thin films made via deposition and annealing of primary films made via co-evaporation of Cu,Sn,S. The photovoltaic properties of solar cells with CTS films as absorbent layers were then studied in relation to the annealing temperature. A solar cell with the voltage in an open circuit of 248 mV a 570°C annealed CTS thin film. A current density in a short circuit of  $33.5 \text{ mA/cm}^2$ , the factor of fill 0.439, and a transformation efficiency of 3.66% [36].

**Dong et al., (2015):**  $\text{Cu}_2\text{SnS}_3$  Sulfurizing stacked metallic precursors yielded CTS thin sheets. and sputtering them by a radio frequency magnetron, according

to this study. The synthetic, structural, morphological, optical, plus electrical characteristics of  $\text{Cu}_2\text{SnS}_3$  thin films formed up soda-lime glass substrates are influenced by the sulfur temperature. The synthetic study reveals totally of the samples remain Sn- rich. Within increasing sulfurization temperatures, the Cu/Sn ratio approaches the stoichiometric composition of CTS. According to structural characterization,  $\text{Cu}_2\text{SnS}_3$  thin films sulfurized by upper sulfur temperatures exhibit greater crystalline kind. At 550 °C for sulfurization, the CTS thin film has a greater amount of crystallization and a bigger average grain size. bandgap is roughly 1.0 eV, as shown by the transmission plus reflectance spectra, compatible with the projected estimate based on outer quantum efficiency. The photoelectric characteristics from solar cells improve as the sulfurization temperature rises. For an area of 0.16 cm<sup>2</sup>, the solar cell produced by the  $\text{Cu}_2\text{SnS}_3$  absorber stratum annealed by 550 °C achieves a 0.28% efficiency [37].

□ **ana□ et al., (2015):**  $\text{Cu}_2\text{SnS}_3$  thin films have been characterised as the result of annealing after co-evaporation of Cu, Sn, and cracked sulphur. Now a quick thermal treating oven supplied by N<sub>2</sub> gas on air pressure, the as-deposited films by annealed at 570 °C for 5 minutes in the of attendance 100 mg of sulphurion lumps. After that, the CTS films were utilised such as absorber layers in solar cells, then their efficiency was measured for various Cu/S ncompositional rate . Films through a considerably Sn-rich composition had the largest grain size. The use of a CTS thin film in solar cells by a (Cu/Sn) rate of nearly 1.9 had the best performance. The voltage across the open circuit of cell by a Cu/Sn rate of 1.87 was 258 mV, the current density in a short circuit was 356mA/cm<sup>2</sup>, the factor of fill was 0.467 plus power transformation efficiency was 4.29 % [38].



Li et al., (2011): in this research demonstrates the use of small -cost metal stannate-founded nanostructures as fast materials for great- fulfillment UV photodetectors. Thin-film devices embrace of amorphous  $\text{ZnSnO}_3$  nanotubes and/or polycrystalline  $\text{Zn}_2\text{SnO}_4\text{-SnO}_2$  nanoparticles by diverse optical plus electrical architectures were successfully produced using a durable, affordable, and scalable drop-casting approach. Thermal treatment from amorphous  $\text{ZnSnO}_3$  nanocubes resulted in the formation of  $\text{Zn}_2\text{SnO}_4\text{-SnO}_2$  heterojunction nanoparticles. Big-area, regular, and continuous film photodetectors by clear plus quick responses, with rise and decay durations smaller than 1.0 s, have been developed when subjected to UV irradiation 370 nm. When compared to their predecessors, these two stannate nanostructures have more benefits, for example  $\text{ZnO}$ ,  $\text{SnO}_2$ ,  $\text{Zn}_2\text{SnO}_4$ ,  $\text{ZnO-SnO}_2$  single nano structures or film photo sensors, containing photo-sensitivities that are extremely high ( $S > 10^2$  and  $\sim 10^3$  existed completed for ( $\text{ZnSnO}_3$ ) and  $\text{Zn}_2\text{SnO}_4\text{-SnO}_2$  photodetectors, respectively then excellent responsivite (as great as  $0.5 \text{ A W}^{-1}$  at 5.0 V bias of the  $\text{Zn}_2\text{SnO}_4\text{-SnO}_2$  photo sensors) below short light intensity [39].

Duan and Li (2011): Have successfully synthesized  $\text{Cu}_2\text{SnS}_3$  (CTS) thin-film deposition employing a spin coating method. The films feature a tetragonal crystal structure, according to XRD. The film form and particle size were then determined using SEM. The crystal's various planes were examined using TEM. Its excellent absorption coefficient of  $10^4 \text{ cm}^{-1}$  and optimum band gap of 1.23 eV enable its use as photoactive material. The visible and infrared (IR) photoresponses were examined at various light intensities. At 3V applied bias, the current increased from a dark current of 0.31 A to 1.78 A at 1.05 suns and 8.7 A under  $477.7 \text{ m W/cm}^2$  IR illumination intensity. At 1.05 lights, the responsivity, sensitivity, outer efficiency in quantum, Then it was revealed

that specific detectivity exists. (10.93 mA/W, 5.74 and 2.47) %, plus  $3.47 \times 10^{10}$ , respectively, while at 477.7 m W/cm<sup>2</sup> IR illumination, they were 16.32 mA/W, 27.16 and 2.53 percent, and  $5.10 \times 10^{10}$  Jones, respectively. The transient photoresponse was measured using visible and infrared illumination [40].

**Lee et al., (2011):** CuZnS is a novel potential element for thin-film photovoltaics that is plentiful and ecologically kindly, according to the report. Copper and Zinc atom ratios may be changed to control electrical and optical characteristics, making it suitable for use as an absorber or window layer. This material's conductivity may be altered of n to p by changing the Cu/Zn rate. The current study shows that raising the Cu to Zn ratio in CuZnS improves the cell characteristics of the CuZnS/In<sub>2</sub>S<sub>3</sub> hetero junction significantly. Current density rise of 5.4 mA/cm<sup>2</sup> to 10.7 mA/cm<sup>2</sup>, improving transformation efficiency of 1% to 1.95%. Results are clear based by the enhancement from several band structures [41].

**Li et al., (2011):** have reported that extremely crystallized CTS thin films by prepared via sputtering-based on deposition. Furthermore, the impact from various annealing temperatures by the crystallographic, electrical, Cu<sub>2</sub>SnS<sub>3</sub> thin films were investigated for their optical characteristics. XRD from the (112), (220), and (312) planes reveal such the produced Cu<sub>2</sub>SnS<sub>3</sub> thin films include a monoclinic structure. Extrapolating from external quantum efficiency (EQE) measurements, the direct bandgap energy of Cu<sub>2</sub>SnS<sub>3</sub> thin film annealed at 580 °C is 1.03 eV. The CTS-based thin-film solar cells (TFSCs) are invented by a structure of Mo/CTS/CdS/i-ZnO/AZO/Al. 1.35% of initial power-transformation efficiency with a (28.3 mA/cm<sup>2</sup>) of current density in a short circuit was

obtained. An voltage in the open circuit. and the factor of fill were found to be 147.5 mV and 32% , respectively [42].

**Lee et al., (2010):** Reported a mono-crystalline CdTe/MgCdTe binary - CuZnS hole contact in a heterostructure solar cell an ITO electrode had been published. Other contact materials, such as a-Si:H or ZnTe, have been used in similar devices to achieve highet open-circuit voltages and low circuit current densities.  $Cu_x Zn_{1-x} S$  is a tunable material system that was synthesized by chemical bath deposition (a low-cost deposition process) and offered a variety of band gaps, conductivity, and band offsets. Devices with  $x = 15\%$ ,  $25\%$ , and  $65\%$  copper compositions have been created and analyzed, producing a top active-area power transformation efficiency of  $12.9\%$ , an voltage in an open circuit of 956 mV, the factor of fill  $63.5\%$ , and a low current density in the circuit from  $21.2 \text{ mA/cm}^2$  [43].

**Li et al., (2010):** In this research. A thin coating of (CZS) for a solar cell was successfully prepared using a pyrolysis by spray preparation process. XRD, UV, SEM, and the J–V tester were used to study the impact of changing the spray temperature of the substrate on the structural, optical, compositional, morphological, and photovoltaic characteristics of the generated CZS film. Under ideal conditions, our unique CZS thin films include a perfect crystallinity phase with a band gap of 2.21 eV and transformation efficiency of  $0.84\%$  , as evidenced by the results [44].

**Lee et al., (2010):** In this work, a transparent conductive made an (oxide/mesoporous)  $Zn_2SnO_4$ . Thermal evaporation is used to place various types of metal oxide semiconductor thin films (such as  $SnO_2$ ,  $TiO_2$ , and ZnO) on the FTO substrate to reduce charge recombination at the synthesized

material interface and increase photovoltaic performance. The results show that, compared to SnO<sub>2</sub> and (ZnO), the TiO<sub>2</sub> thick layer is the best effective obstructive layer to suppressing recombination of charges and boosting the constructed devices current density in a short circuit and power conversion efficiency. Furthermore, the creation of an energy barrier at the FTO/Zn<sub>2</sub>SnO<sub>4</sub> contact results in the formation of an energy barrier, The device with the TiO<sub>2</sub> blocking layer achieves With a current density of 7.36 mA/cm<sup>2</sup> in a short-circuit and a voltage in the open circuit of 664 mV, the highest power conversion efficiency is 3.02%. According to this study, Charge recombination at boundary is one of the major problems limiting the power conversion efficiency of dye-sensitized solar cells [45].

□ □ **et al., (201□)**: Using the sol-gel solution approach, they created monoclinic Cu<sub>2</sub>SnS<sub>3</sub> thin films. The influence of the Cu/Sn atomic ratio on structure and morphology have been investigated. The CTS films grew more compact when the Cu/Sn atomic ratio rise from 1.6 to 2.0, minor phases for example SnS faded away, then the grain size of the films reduced. The Cu/Sn ratio of 1.9 in the CTS film resulted in a monoclinic structure and homogenous morphology plus a band gap of 1.12 eV, resulting in a power transformation efficiency of 0.58%. Then, Cu<sub>2</sub>SnS<sub>3</sub> (CTS) can be considered a possible thin-film solar-cell material [46].

□ □ □ □ □ □ □ □ **et al., (2020)**: The application of heterogeneous Cd<sub>2</sub>SnO<sub>4</sub>/CdS/Cu<sub>2</sub>O/Ag in solar cells was researched by the researcher. Chemical procedures were used to deposit the heterostructure on the glass substrate: (1) Sol-gel synthesis of Cd<sub>2</sub>SnO<sub>4</sub> as TCO, (2) Chemical bath deposition of CdS as an n-layer, and (3) Cu<sub>2</sub>O as the player via pyrolysis by spray . The Cd<sub>2</sub>SnO<sub>4</sub> and CdS layers have thicknesses of 290 and 135 nanometers, respectively. Cu<sub>2</sub>O (τ)

of various thicknesses was used to investigate the impact of this parameter on solar cell performance (135, 185, 220, 350, and 800 nm). Photovoltaic values at their best remained  $V_{OC} = 346$  mV,  $J_{SC} = 1.57$  mA/cm<sup>2</sup>,  $FF = 33.4$  and  $\eta = 0.18$  percent for  $d = 220$  nm. Gaps in the Cu<sub>2</sub>O plus CdS bands. The current donating is mostly due to flaws in the Cu<sub>2</sub>O lattice, which result in an energy level source inside the band gap [47].

□ **a□□□□□ et al., (2021)**: Using the co-precipitation approach, high-quality Zn<sub>2</sub>SnO<sub>4</sub> nanoparticles were generated, and they were able to improve the degree of crystallization as well as a pure phase of the final nanopowders by varying pH, Temperatures of annealing plus concentrations of precursors. The porous layer was then modified with MgO and Al<sub>2</sub>O<sub>3</sub> passivation layers, after which Zn<sub>2</sub>SnO<sub>4</sub> crystalline nanoparticles by an average size of nearly 35 nm existed utilized as a porous layer. Controlling the solution concentration and spin coating operation speed enhanced the thickness of these barrier layers, which was critical in reducing recombination by significantly improving the showing of DSSCs. The electronic settings with the highest values were obtained for  $J_{SC} = 8.59$  mA/cm<sup>2</sup>,  $V_{OC} = 0.66$  V, and  $FF = 0.51$  for the MgO-treated device with a rotational speed of 4000 rpm, which exhibited a 40% increase in efficiency from 2.07% to 2.90 % as compared to the untreated sample. All of the treated samples showed a reduction in VOCs. Electrochemical resistance spectroscopy, The transport and recombination mechanisms were subsequently investigated using, voltage in open-circuit decay, and the dye loading procedure, which confirmed a higher transfer ratio and slower electron recombination in the greatest modified devices [48].

Deeb, and Alkhatib, (2021): Zinc Stannite  $Zn_2SnO_4$  nanoparticles were synthesized using a solvent and heat technique, according to the study. XRD analysis reveals that the nanoparticles generated have a face-centered cubic spinel shape. According to TEM pictures, the produced  $Zn_2SnO_4$  nanoparticles are roughly 20 nm in size. To prepare photoanodes for use in semi-transparent dye sensitized solar cells, a paste incorporating synthetic  $Zn_2SnO_4$  nanoparticles was developed. Semi-transparent dye-sensitized solar cells based on dye adsorbed  $Zn_2SnO_4$  photoanodes have a photoconversion efficiency of 0.86% [49].

### 1.10 Objective:

1-Synthesis of some different ternary metal oxides and sulfid  $Cd_2SnO_4$  (CTO),  $Zn_2SnO_4$  (ZTO),  $Cu_2SnS_3$  (CTS), and  $CuZnS$  (CZS) thin films using different method (chemical spray pyrolysis, spin coating, sol-gel and drop-casting methods)

2-Study effect of substrates temperature on the structure, Morphological, Optical and electrical properties of prepared thin film.

3-Synthesis of  $Cd_2SnO_4$  (CTO),  $Zn_2SnO_4$  (ZTO),  $Cu_2SnS_3$  (CTS), and  $CuZnS$  (CZS) nanoparticle by sol-gel method.

4-Applications of prepared thin films in photovoltaics applicable such as solar cell and photodetectors.